# A DUAL-BAND ANTENNA ENABLED USING A COMPLIMENTORY SPLIT RING RESONATOR (CSRR) PLACED IN THE GROUND PLANE

A Thesis
Submitted to the Graduate Faculty
of the
North Dakota State University
of Agriculture and Applied Science

By

Ruisi Ge

In Partial Fulfillment of the Requirements
for the Degree of
MASTER OF SCIENCE

Major Department:
Electrical and Computer Engineering

January 2019

Fargo, North Dakota

# North Dakota State University
Graduate School

**Title**

A DUAL-BAND ANTENNA ENABLED USING A COMPLIMENTORY SPLIT RING RESONATOR (CSRR) PLACED IN THE GROUND PLANE

**By**

Ruisi Ge

The Supervisory Committee certifies that this ***disquisition*** complies with North Dakota State University's regulations and meets the accepted standards for the degree of

**MASTER OF SCIENCE**

SUPERVISORY COMMITTEE:

Benjamin Braaten
Chair

Jacob Glower

Mijia Yang

Approved:

1/31/2019
Date

Benjamin Braaten
Department Chair

## ABSTRACT

The microstrip patch antenna is regarded as one of the key components for compact, low cost RF communications and wireless power techniques. In some instances, there are requirements that a system communicate on a different band than the wireless power harvesting band. To address these multi-frequency, a novel dual-band patch antenna enabled with complementary split ring resonators (CSRRs) is designed and fabricated. This antenna operates at 2.4Ghz and 915 MHz, and the antenna miniaturization is achieved by etching the complementary split ring resonators (CSRRs) in the ground plane. A prototype antenna is fabricated and tested, and measured results are in good agreement with simulations. Furthermore, the influence of the CSRR on the behavior of the antenna is also explored and discussed.

## ACKNOWLEDGEMENTS

First, I would like to thank my advisor, Dr. Benjamin Braaten, for his encouragement, guidance, and patience for this research. Dr. Braaten's office was always open whenever I ran into a trouble spot or had a question about my research or writing. Without his support I would never successfully complete as much as I did.

I would also like to thank my committee members Dr. Jacob Glower. Dr. Jacob Glower is always patient when I have question about the research and he gave me so many useful suggestions.

I would like to thank to my lab mates Ryan Striker and Jerika Cleveland. Jerika gave me many helpful suggestions for HFSS simulations and Ryan help me to mile the prototypes.

## TABLE OF CONTENTS

## LIST OF TABLES

## LIST OF FIGURES

## LIST OF SYMBOLS

Pr ..... Received Power

$\lambda$ ..... Wavelength

*R* ..... Distance

*Gt* ..... Gain of transmitting antenna

*Gr* ..... Gain of receiver antenna

# CHAPTER 1. INTRODUCTION

## 1.1. Motivation

Recently, there has much research interest in utilizing radio frequency (RF) harvesting techniques to power up the next generation wireless sensor networks. As compared to other energy harvesting techniques such as solar [2], vibration [3], and thermal [4], RF energy does not rely on ambient sources that are beyond control in many situations. This enables an RF energy harvester to have the potential to work in many places where a dedicated RF power source can be provided.

One challenge for far field RF harvesting though is the low efficiency, and sometimes, the harvested power is not sufficient to support wireless node operate consistently over a long distance. Researchers have tried to solve this issue by two main approaches: (1) improve the efficiency of the transmitted and receive antenna and (2) improve the energy storage option to better reserve energy. To add to these approaches, a CSRR patch antenna designed in this thesis to better receive RF energy with a compact size. A RF-Power wireless sensor node along with a non-ideal supercapacitor storage estimate model is also proposed for improved RF energy reserve.

## 1.2. RF-Powered Wireless Sensor Networks

WSNs are a set of devices placed in different locations on the environment to monitor one or more physical conditions such as temperature, humidity, acceleration, etc. WSNs usually cooperatively transfer monitoring data through the network to a data station. With the development of semiconductor technology, WSNs have attracted more attention from both industry and academia due to their advantages such as convenience, low power, and low cost.

In RF energy harvesting, the near field techniques include inductive coupling [5] and magnetic resonance coupling [6]. Both two techniques require calibration and alignment of coils/resonator at transmitter and receivers [7]. Even employed with high power density and high

conversion efficiency, the power strength is attenuated according to the cube of the reciprocal of the distance [8]. The far-field energy harvesting, however, uses antenna to receive the RF signal.

One big disadvantage of this technique is the inconsistent power supply during the data transmission. For example, inconsistent power could interrupt the handshaking process. Without the handshaking process, wireless sensor devices are unable to recognize each other dynamically. Dynamic network discovery mechanisms are critical for internet of things (IoT) applications. It enables the interaction between devices that are not pre-configured [9]. Thus, it is necessary to find a power source to support constant power during the handshaking process.

### 1.3. CSRR Patch Antenna

The antenna is regarded as one of the key components for compact, low cost wireless sensor nodes. To achieve harvesting RF power, and broadcasting high quality signals with a small footprint, the antennas need to handle multiple band signals. As compact size is a key metric for wireless sensor nodes, antenna miniaturization becomes a very important task to achieve an optimal design for such nodes. Cost is another important aspect for such antennas, considering in practice, hundreds of those nodes need to be deployed in environment.

Microstrip patch antennas have been widely used due to their low cost and ease of fabrication [10]. However, they are rarely used on wireless sensor nodes due to their large dimensions at lower frequencies. Many researchers have proposed multiple methods to achieve antenna miniaturization for patch antenna [5] [6]. Among all the methods, special attention has been devoted to utilizing split ring resonators (SRRs) with patch antennas. More recently, complementary split-ring-resonators (CSRRs) have grown as one of the more promising techniques for antenna miniaturization.

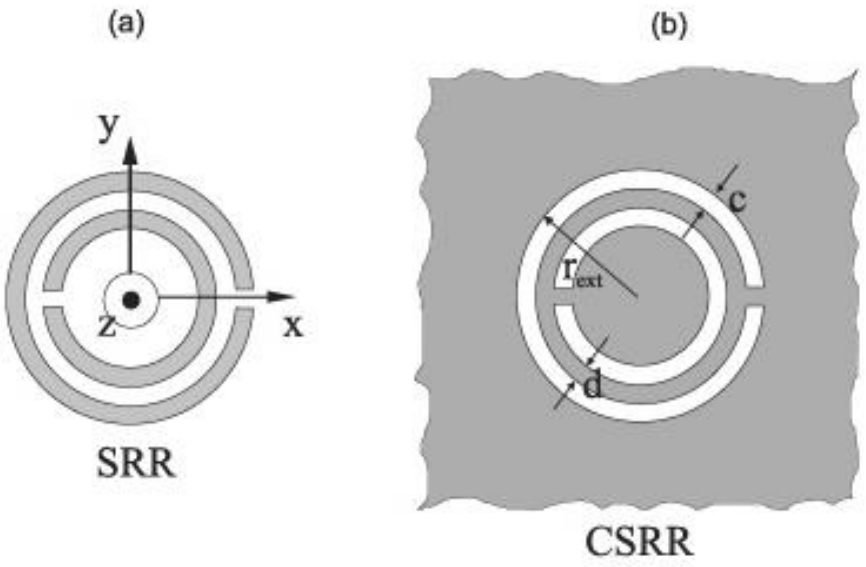


Figure 1. Geometries of the SRR and the CSRR [11]

Examples of geometries of the SRR and the CSRR are show in the Fig 1 [11]. A CSRR is a complement image of split-ring resonator (SRR). In a patch antenna, it is implemented by removing the copper in the shape of a SRR from the ground plane. When the current flowing along the CSRR coils, voltage gradients occur between the CSRR gap and inductance [12]. The CSRR can interact with the electric field, therefore changes the effective permittivity around the resonant frequency. A dual-band characteristic can also be obtained after implementing the CSRR.

A compact dual-band microstrip patch antenna loaded with a CSRR is designed and fabricated here. The proposed antenna is designed to operate at the dual frequencies of 915 MHz and 2.4 GHz. A Rogers TMM4 substrate with a thickness of 1.6mm is used on this antenna. By implementing a CSRR on the ground plane, a 23% size reduction for the patch is achieved compared to a conventional patch antenna. With a dual-band frequency center at 915 MHz and 2.4 GHz, this antenna design is a better option for RF energy harvesting compared to other CSRR antenna designs. Furthermore, the performance influence of the CSRR is discussed.

## 1.4. Thesis Organization

This work is divided into 4 chapters. The first chapter is the motivation and introduction. Chapter 2 provide the detail of RF-powered wireless sensor node and a non-ideal supercapacitor storage estimate model. Chapter 3 presented a dual-band patch antenna with complementary split ring resonators (CSRRs) for RF-powered wireless sensor node. The CSRR'S influence on the patch antenna's performance is also discussed. The final chapter gave the conclusion and future work.

## CHAPTER 2. RF-POWERED WIRELESS SENSOR NODE

### 2.1. Wireless Sensor Node Overview

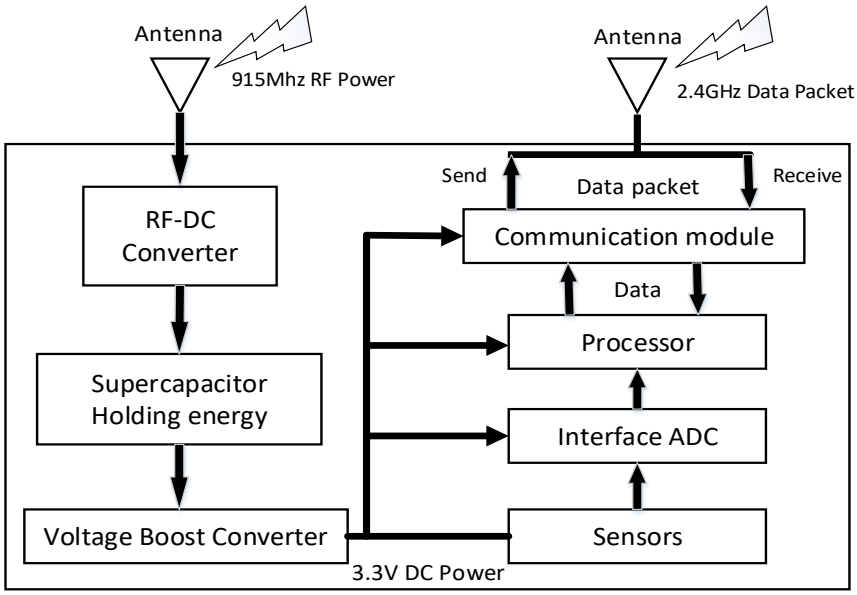


Figure 2. Function block diagram

The block diagram of the wireless sensor node is show in the Fig. 2. This wireless sensor node includes RF to DC converter, a capacitor, DC voltage boost converter, voltage monitor, processor and a 2.4 GHz communication module. RF energy is harvested from the air through the antenna on this sensor node. The converted DC energy is store in a supercapacitor. The voltage on the capacitor will be internally clamped if the harvest energy becomes too large [13]. The RF to DC voltage converter keeps charging the supercapacitor until it reaches a charge threshold. The voltage boost converter then boosts the voltage to the required output voltage level.

The wireless sensor node needs to operate at a relatively low power while having the ability to support dynamic network discovery mechanisms. Therefore, microchip and RF transceiver are chosen for low power purposes.

## 2.2. RF Energy Estimate

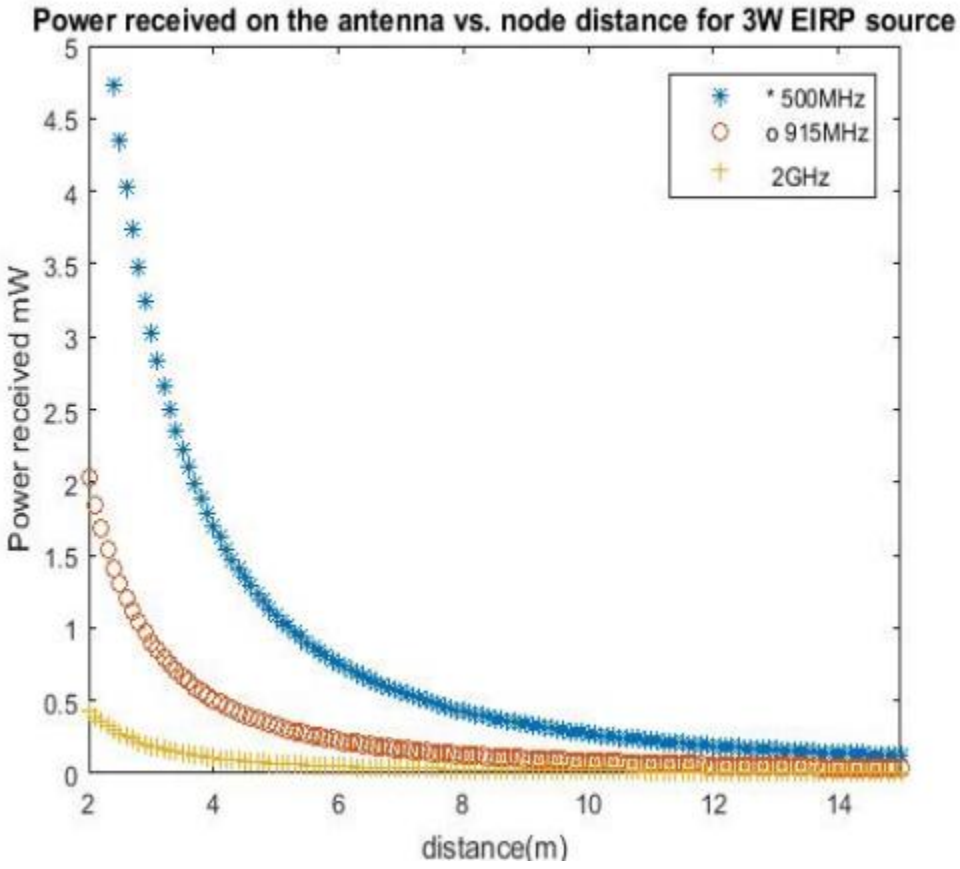


Figure 3. Theoretical RF power received at three different frequency

For this work it is assumed that the power supply for the end device is the RF energy harvested from a dedicated far-field source. Therefore, it is important to estimate the RF energy received. For far field RF power transmitting, the received power is estimated by the Frris equation [14]:

$$\frac{P_r}{P_t} = \left(\frac{\lambda}{4\pi R}\right)^2 G_t G_r \qquad (1)$$

Where *Pr* is the received power, $\lambda$ is the wave length of the RF signal, *R* is the distance between the antennas, *Gt* is the gain of transmitting antenna, and *Gr* is the gain of receiver antenna, and *R* should be much greater than wave length (i.e. far-field).

Next, suppose we have a 3W EIPP, 6 dBi transmitted and received gain, then in theory, the power received at three different frequencies at difference distances is show in Fig 3. As we can see, with lower frequency, the receive power increases. In practice, the lower frequency will more likely be absorbed by obstacles, therefore RF power frequency is at 915MHz.

# CHAPTER 3. CSRR PATCH ANTENNA

## 3.1. Dual-band CSRR Patch Antenna Design Parameter

The geometry of the proposed dual-band CSRR patch antenna design can be seen in Fig. 4. A Rogers TMM4 substrate with a relative permittivity of 4.5 and thickness of 1.6 is used in this design. The patch design on the top will fit well within a 100x100 $mm^2$ substrate. A conventional patch with dimensions of 65x90 $mm^2$ is implemented on the top side. A CSRR is etched out on the ground plane to reduce the resonant frequency.

This dual band CSRR patch antenna is designed to have operating frequencies of 915Mhz and 2.4Ghz. Most ZigBee/IEEE 802.15.4 based wireless sensor networks operate in the 2.4-2.4835 GHz band [15], therefore it's important to have it as a communication band for wireless sensor networks.

During the design process, the antenna is tuned to resonate at 2.4 GHz and 915 MHz by adjusting the dimensions and positions of the patch and CSRR using the commercial software HFSS. The rectangular patch is positioned at the center of the top substrate. This patch is fed through a microstrip line connected to a SMA connector. The feedline has a length of 57.5 mm and width of 2.8 mm which gives a characteristic impedance of 50 Ω. There is also a notch alongside the feedline to improve the signal strength. The width of the notch is 3.1 mm.

On the ground plane, a CSRR is etched out to shift the frequency. There is one outer square and one inner square complement to each other. The width of each square is 2.5mm, while the side length of the outer square and inner square is 37.0 mm and 27.0 mm, respectively. There are two similar gaps etched out for the outer square and inner square in opposite directions. The gap length is 8.8mm. The center of this CSRR is 9 mm away from the patch center in the horizontal direction.

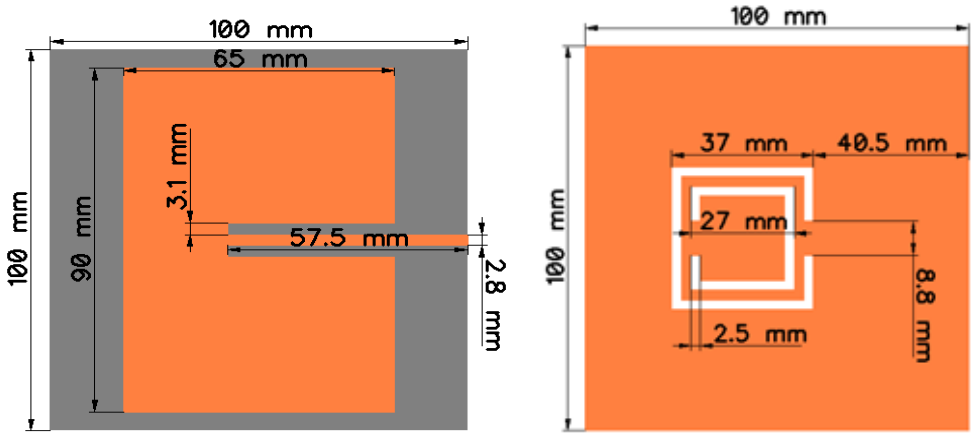


Figure 4. Geometry of the CSRR dual-band patch antenna: (a) top view and (b) bottom view

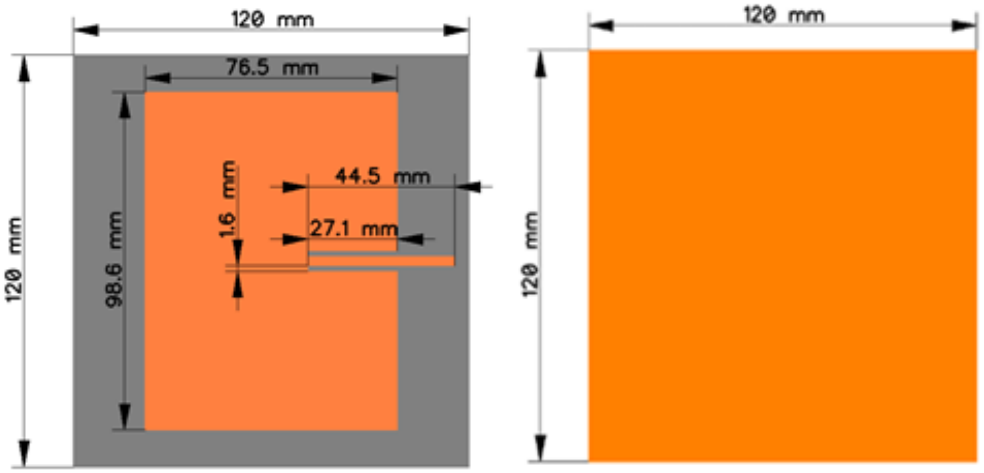


Figure 5. Geometry of the conventional patch antenna: (a) top view and (b) bottom view

As a comparison for the proposed CSRR patch antenna, a conventional patch antenna is designed to work at 915 MHz, as show in the Fig 5. The same Rogers TMM4 substrate with the same height is applied to this conventional patch antenna. Similar to the proposed CSRR patch antenna, the patch and feedline is implemented on the top of a 120x120 $mm^2$ substrate, while the ground is placed underneath the substrate. The dimension of the antenna patch's dimensions are 98.6mm x72.5 mm, with a 44.5mm feedline. The width of the notch is 1.6 mm. The ground plane does not have a CSRR. For further comparison, the dimension differences are listed in the TABLE I:

Table 1. CSRR Patch and Conventional Dimension

| Patch Dimension Comparison | | |
|---|---|---|
| Parameter (mm) | CSRR | Conventional |
| Substrate Length | 100 | 120 |
| Patch Length | 90 | 98.6 |
| Patch Width | 65 | 76.5 |
| Feedline Length | 57.5 | 44.5 |
| Feedline Width | 2.8 | 2.8 |
| Gap | 3.1 | 1.6 |

Table I shows there is approximate 23 % patch size reduction, and 17% size reduction for the total substrate.

### 3.2. Simulation and Test Results

The antenna proposed in the previous section was first designed and simulated in Ansys HFSS [16]. The prototypes were fabricated later on a Rogers TMM4 substrate. The fabricated antenna is shown in the Fig 6. Fig 6(a) shows the top layer of the antenna, and Fig 6(b) shows the ground plane where a CSRR ring is etched out. The reflection coefficient of the fabricated antenna is measured using the Keysight E5071C Network Analyzer. The results obtained from the simulation and measurement of the Dual-band CSRR patch antenna are summarized in the following section:

Figure 6. Fabricated dual-band CSRR patch antenna: (a) top layer and (b) bottom layer

### 3.2.1. Reflection Coefficient

The simulations and measured reflection coefficients for this dual-band CSRR patch antenna are shown in Fig 7. It is shown that the antenna resonates at 915 MHz and 2.41 GHz. The simulated reflection coefficient is -20 dB at 915 MHz, and -19.1 dB at 2.4 GHz. The bandwidth is around 50 MHz for 915 MHz and 2.4 GHz.

The measured results for the fabricated antenna show a close agreement with the simulated ones. The measured reflection coefficient is -16.13 dB and -21.02 dB at 915MHz and 2.4 GHz, respectively. There is a minor bump in the graph which shows at 2.2 GHz, however, the reflection coefficients for simulations and measurements for 915MHz and 2.4 GHz are only -7.3 dB and -8.5 dB, respectively. It is less than -10 dB. Therefore, it won't have a big influence on performance. It is worth mentioning that the conventional patch antenna resonates only at 915 MHz with reflection coefficient of -30.6 dB. The overall gain of the proposed antenna is lower than the conventional patch antenna at 915 MHz. The presence of the CSRR on the ground plane dissipates part of the power to resonate at higher frequencies and therefore affecting lower band gain.

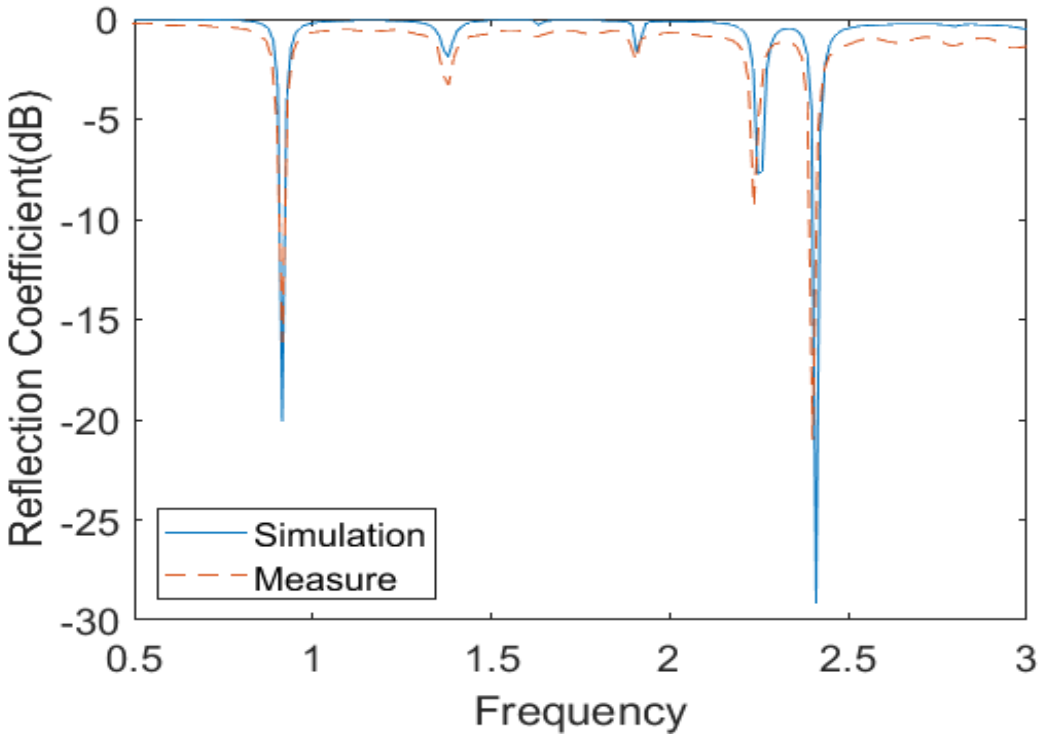


Figure 7. Reflection coefficient of dual-band CSRR

### 3.2.2. Current Distribution

The current distribution for the CSRR patch antenna on both the patch and ground at 915 MHz and 2.4 GHz are shown in Fig 8. The high current levels on the edge indicate good radiation. As a comparison, the current distribution for a conventional patch antenna is shown in Fig 8. From observation, at the lower frequency of 915 MHz, the current distribution of the proposed CSRR antenna is very similar to the conventional patch antenna. At the higher frequency, however, the current distribution of the proposed CSRR antenna is very different than the convention patch antenna.

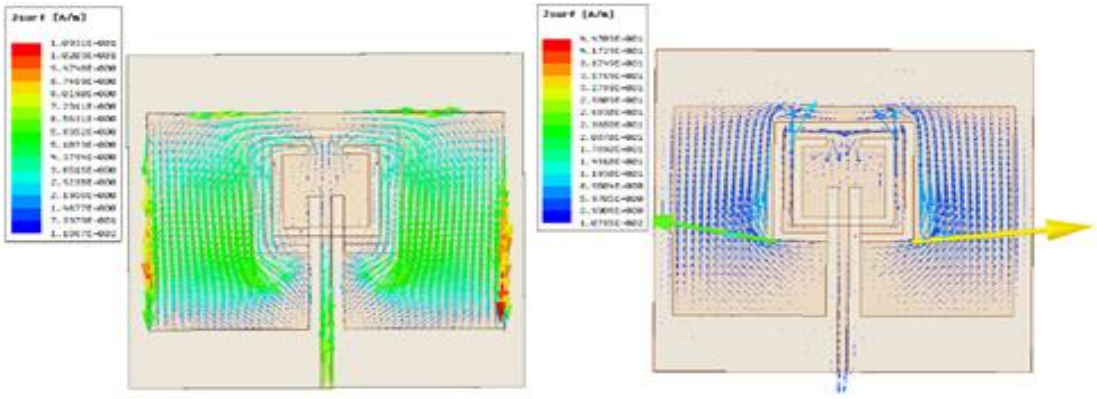

(a) Dual-band patch CSRR Antenna at 915 MHz

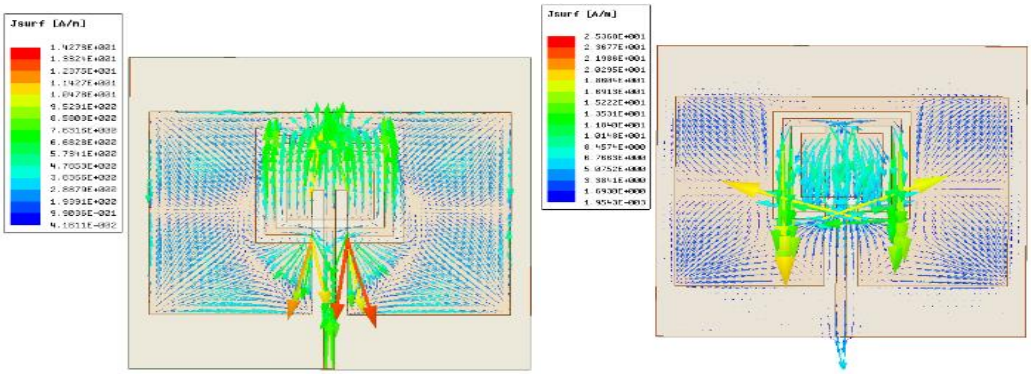

(b) Dual-band patch CSRR Antenna at 2.4 GHz

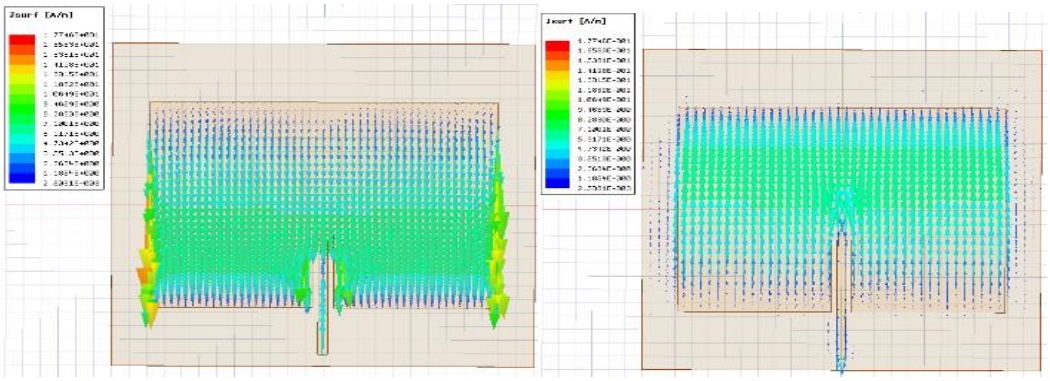

Figure 8. Current distributions on the patch (left) and ground plane (right). (a) Dual-band patch CSRR Antenna at 915 MHz (b) Dual-band patch CSRR Antenna at 2.4 GHz (c) Convention Patch Antenna at 915 MHz

One assumption is the lower 915 MHz band is inspired by the patch, while the higher 2.4 GHz band is determined by the CSRR. After adding the CSRR to the ground plane, the current of the patch is rearranged. At lower frequencies, the patch size is the main factor for the resonate

frequency. Due to the coupling between the CSRR and the patch, this frequency shifts to a lower band. Therefore, antenna miniaturization can be achieved by adjusting the CSRR dimensions. At higher frequency, when the CSRR dimensions become the main factor, a second band of 2.4 GHz is produced.

### 3.2.3. Radio Pattern

The simulated radiation pattern of the designed antenna in the far-field is plotted in dB and it shown in Fig 9, as we can see at phi =0, and phi = 90. This pattern shows that the max gain is around 2.0 dB. In addition, the 3-D radiation pattern in dB is show in Fig 10.

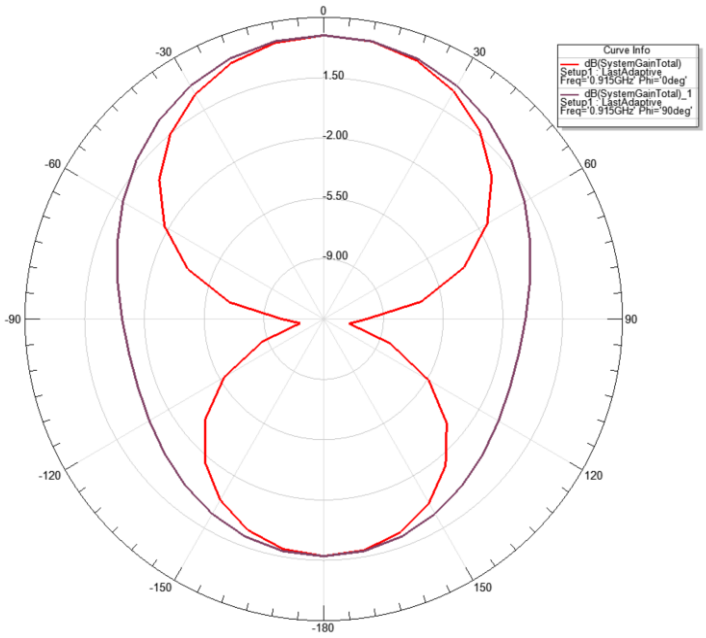


Figure 9. Radio pattern of antenna gains at Phi=0 and Phi = 90 degree

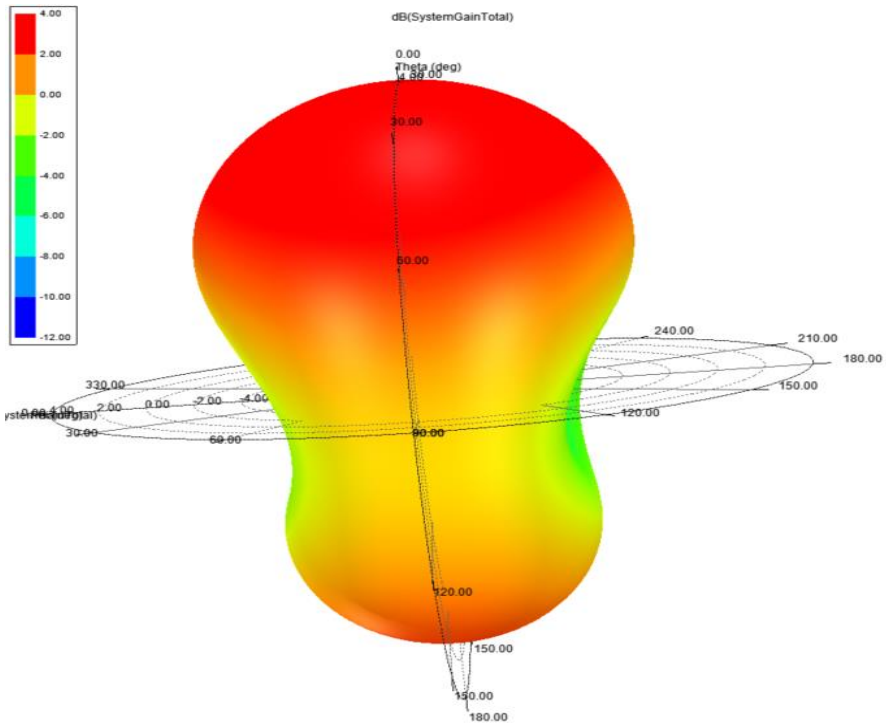


Figure 10. 3D radiation pattern in dB at 915MHz

### 3.3. CSRR Patch Antenna With Improved Gain

Next Fig 11 shows the geometry of a modified CSRR antenna design. The main purpose of this design is to improve the overall gain of the CSRR patch antenna. As we already showed, the previous design, the reflection coefficient has a good match between the simulation and measurement results. However, the CSRR antenna overall gain is smaller compared to the traditional patch antenna. Therefore, it is important to improve the overall gain for the CSRR patch antenna.

We added two slots on top of the original CSRR patch antenna design. Based on the HFSS simulation result, we have also adjusted the overall dimension of the patch size to center the frequency to 915Mhz and 2.4Ghz. The new dimension compared to the previous CSRR patch antenna is show in table II.

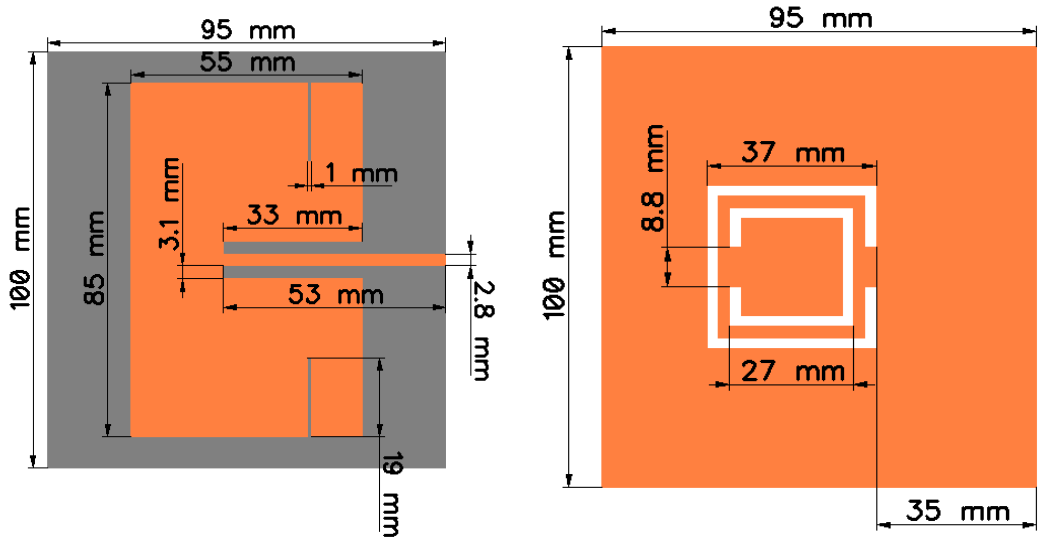


Figure 11. Geometry of the CSRR dual-band patch antenna: (a) top view and (b) bottom view

Table 2. CSRR Slot Patch and Original Dimension

| Patch Dimension Comparison | | |
|---|---|---|
| Parameter (mm) | Original CSRR | CSRR Patch with Slot |
| Substrate Length | 100 | 95 |
| Patch Length | 90 | 85 |
| Patch Width | 65 | 55 |
| Feedline Length | 57.5 | 53 |
| Feedline Width | 2.8 | 2.8 |
| Gap | 3.1 | 1.6 |
| Slot Position | None | -15 |
| Slot length | None | 19 |

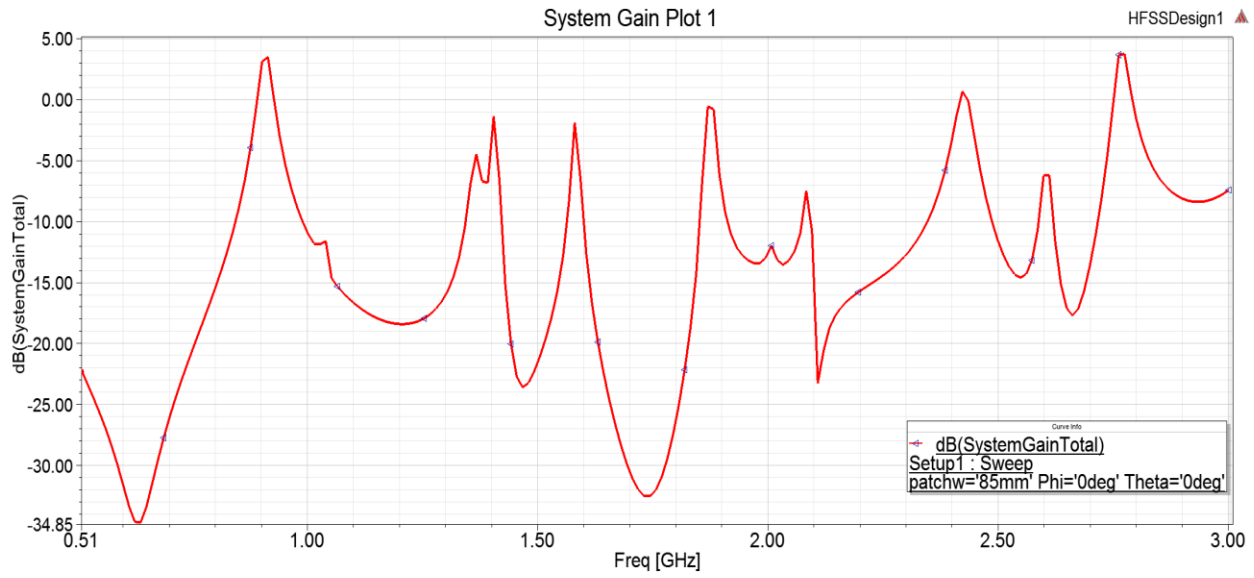


Figure 12. Modified CSRR Patch Antenna Gain (dB)

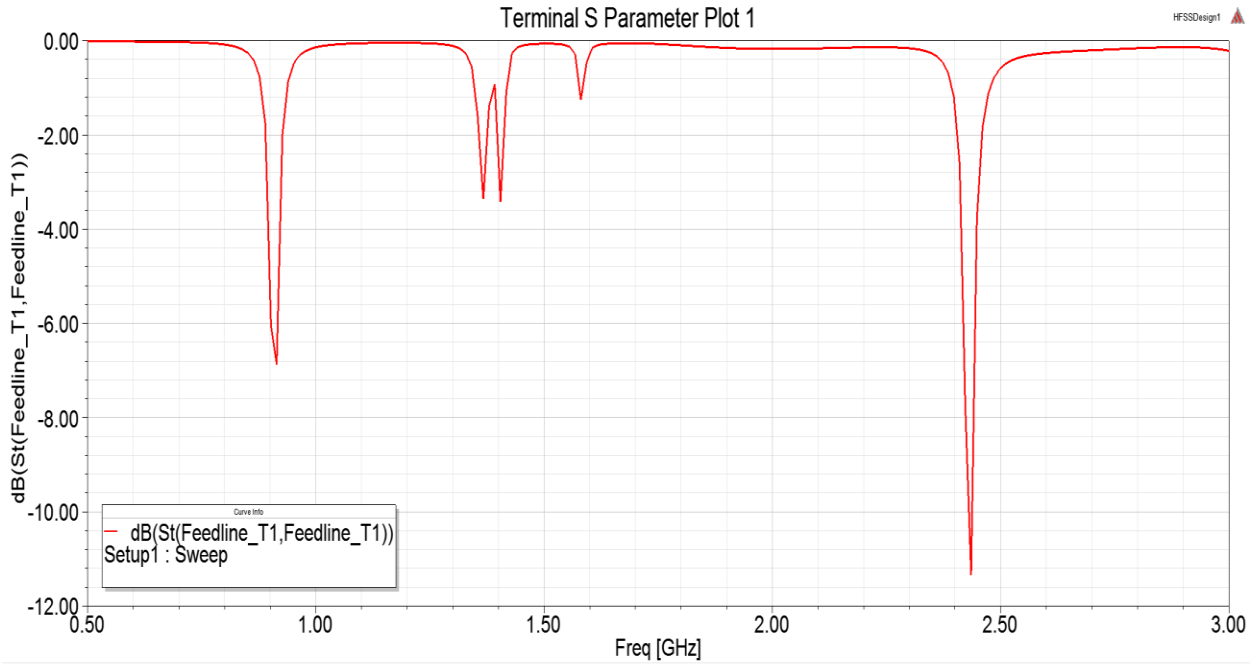


Figure 13. Reflection coefficient of Modified CSRR Patch Antenna

From table II, we can see that the overall dimension reduces compared to the original CSRR. The antenna gain showed an improvement for 915MHz and 2.4 GHz, however, the simulated reflection coefficient has shown a decrease. The result are shown in Fig 12 and Fig 13.

### 3.4. CSRR's Influence To Antenna Performance

#### 3.4.1. CSRR Size and Position

In this section, we are exploring different CSRR sizes and location's and how they influence the patch antenna. In the first case, a larger CSRR is etched out from the ground plane. Compared to the original design, the CSRR is moved 4 mm away from the patch center instead of 9 mm. Fig 14 presented the reflect coefficient comparison of those three simulations. Compared to the original antenna design, the larger sized CSRR moved the higher band to a lower value of 2.171 GHz. The lower band resonate frequency slightly shifts to 902 MHz. It is clearly shown that the size of the CSRR has more influence on the higher frequency band. This result further verifies our previous assumption that the higher band is mainly produced by the CSRR.

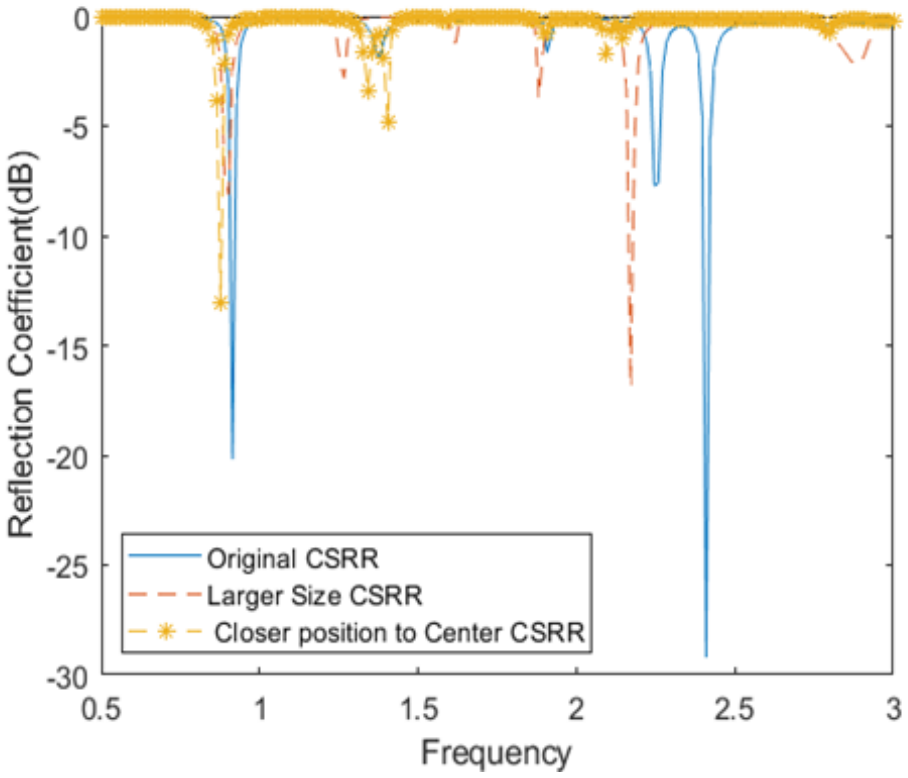


Figure 14. Reflection coefficient of (a) original CSRR design (b) large size CSRR (c) closer position to patch center CSRR

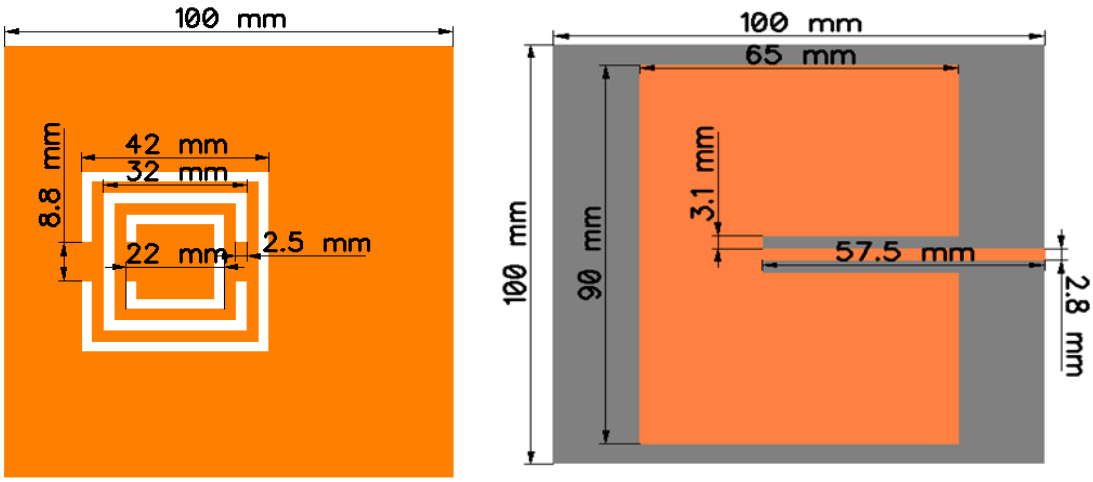


Figure 15. Geometry of the 3-ring CSRR patch antenna: (a) top view and (b) bottom view

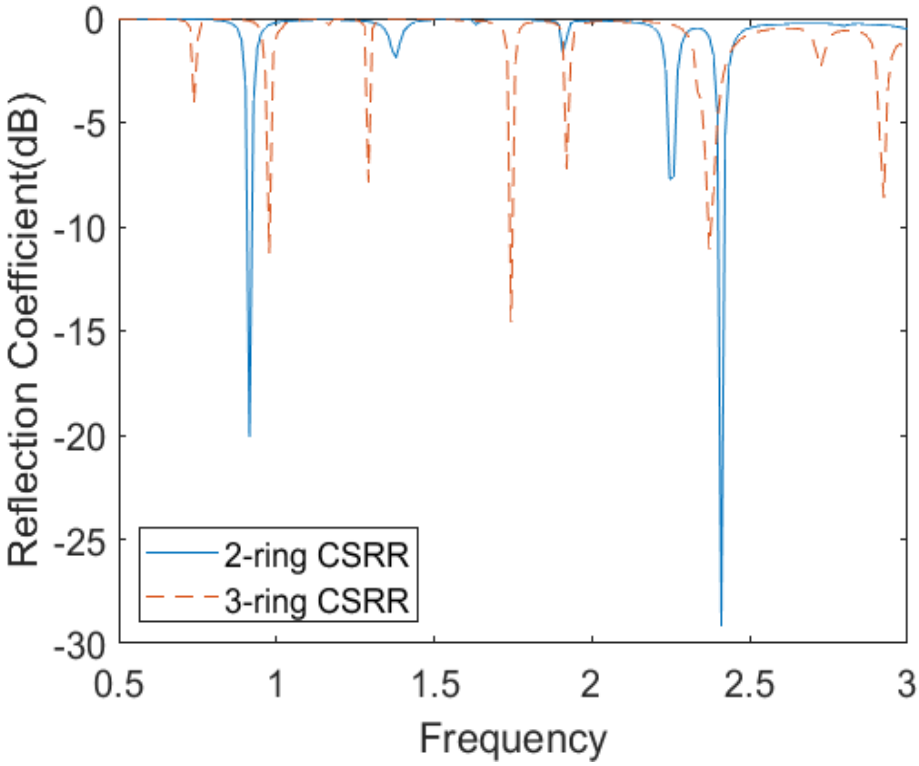


Figure 16. Reflection coefficient of (a) original CSRR design (b) 3-ring CSRR

Comparing the reflection coefficient of the third design with the original design, the higher frequency band no longer exists. The lower band center frequency further shifts to 876 MHz. One possible explanation is that the CSRR starts interfering with the patch's notch on the top when it

is close to the center. The CSRR no longer creates a higher band, instead it rearranges the surface current and causes the lower band to shift to a lower center frequency.

### 3.4.2. Multiple Ring Influence

To further verify the assumption that the CSRR will result in a new frequency band, a multi-ring CSRR is designed and simulated in HFSS as a comparison result to the original dual-band CSRR patch antenna. In this new design, an extra square is etched out of the ground plane.

Fig 15 shows the geometry of a three-ring CSRR patch antenna. There is a total of 3 squares with the lengths of 42 mm, 32 mm, and 27 mm etched out from the ground plane. The width of the square stays at 2.5 mm. The gap of the square also stays at the same size.

Fig 16 shows the reflection coefficient of the 3-ring CSRR patch antenna. Compared to the original design, the higher band is slightly shifted to 2.37 GHz at -11.1 dB, and the lower band shifts to 977 MHz at -11.3 dB. A new band appeared at 1.744 GHz at -14.58 dB. This result indicates adding more rings, a multiband antenna can be achieved.

# CHAPTER 4. CONCLUSION

In this research, a new dual-band CSRR patch antenna is presented. Proposed for the RF harvesting wireless sensor network application, this antenna is designed to operate at 915 MHz and 2.4 GHz. The antenna was fabricated on a Rogers TMM4 substrate with a patch size of 90x65 $mm^2$. A 23% area reduction was achieved by implementing a CSRR on the bottom of the patch antenna. Good agreement between simulated and measured results validates the design. Finally, the CSRR'S influence to the patch antenna's performance is also discussed.

Further work could be done to explore the CSRR's influence on the patch antenna. The gain of the patch antenna could also be vastly improved. This would allow more power to be harvested. In addition, a more compact RF-powered wireless sensor node can be implemented to deployed on environment.

## REFERENCES


[1] G T. Le, K. Mayaram, and T. Fiez, “Efficient far-field radio frequency energy harvesting for passively powered sensor networks,” IEEE J. Solid-State Circuits, vol. 43, no. 5, pp. 1287–1302, May 2008.

[2] D. Brunelli, L. Benini, C. Moser, and L. Thiele, “An Efficient Solar Energy Harvester for Wireless Sensor Nodes,” in Design, Automation and Test in Europe, 2008. DATE ’08, 2008, pp. 104–109.

[3] K. Vijayaraghavan and R. Rajamani, “Ultra-Low Power Control System for Maximal Energy Harvesting From Short Duration Vibrations,” IEEE Trans. Control Syst. Technol., vol. 18, no. 2, pp. 252–266, Mar. 2010.

[4] R. Grezaud and J. Willemin, “A self-starting fully integrated auto-adaptive converter for battery-less thermal energy harvesting,” in New Circuits and Systems Conference (NEWCAS), 2013 IEEE 11th International, 2013, pp. 1–4.

[5] H. Liu, Maximizing Efficiency of Wireless Power Transfer with Resonant Inductive Coupling, 2011. [Online]. Available: http://hxhl95.github.io/media/ib_ee.pdf.

[6] A. Kurs et al., “Wireless power transfer via strongly coupled magnetic resonances,” Science, vol. 317, no. 5834, pp. 83–86, Jun. 2007.

[7] X. Lu, P. Wang, D. Niyato, D. I. Kim and Z. Han, "Wireless Networks With RF Energy Harvesting: A Contemporary Survey," in IEEE Communications Surveys & Tutorials, vol. 17, no. 2, pp. 757-789, Secondquarter 2015.

[8] J. O.Mur-Miranda et al., “Wireless power transfer using weakly coupled magnetostatic resonators,” in Proc. IEEE ECCE, Atlanta, GA, USA,Sep. 2010, pp. 4179–4186.

[9] D. Bandyopadhyay and J. Sen, “Internet of things: Applications and challenges in technology and standardization,” Wireless Pers. Commun., vol.58, no.1,pp.49–69,2011.

[10] N. Hojjat, F. G. Kharakhili, M. Fardis, G. Dadashzadeh, A. Ahmadi, "Circular Slot with A Novel Circular Microstrip Open Ended Microstrip Feed For Uwb Applications", Progress In Electromagnetics Research PIER 68, pp. 161-167, 2007.

[11] R. Marqués et al., “Ab initio analysis of frequency selective surfaces based on conventional and complementary split ring resonators,” J. Opt. A, Pure Appl. Opt., vol. 7, no. 2, pp. S38–S43, 2005.

[12] M. S. Sharawi, M. U. Khan, A. B. Numan and D. N. Aloi, "A CSRR Loaded MIMO Antenna System for ISM Band Operation," in IEEE Transactions on Antennas and Propagation, vol. 61, no. 8, pp. 4265-4274, Aug. 2013.\

[13] Powercast, “915 MHz RF Powerharvester Receiver,” P2110B datasheet, Nov. 2014.

[14] O. B. Akan, M. T. Isik and B. Baykal, "Wireless passive sensor networks," IEEE Communications Magazine, vol. 47, no. 8, pp. 92-99, August 2009.

[15] Li Xiaoman and Lu Xia, "Design of a ZigBee wireless sensor network node for aquaculture monitoring," 2016 2nd IEEE International Conference on Computer and Communications (ICCC), Chengdu, 2016, pp. 2179-2182

[16] Ansoft Corporation, High Frequency Structure Simulator (HSFF) User Manual, Pittsburgh, PA, Ansoft Corporation, 2001